Hindawi
Advances in Civil Engineering
Volume 2019, Article ID 5630805, 15 pages
https://doi.org/10.1155/2019/5630805

Research Article

Mechanical Performance and Numerical Simulation of Basalt Fiber Reinforced Concrete (BFRC) Using Double-K Fracture Model and Virtual Crack Closure Technique (VCCT)

Yawei Zhao,[1] **Xinjian Sun**,[1] **Peng Cao**,[1,2] **Yifeng Ling**,[3] **Zhen Gao**,[1] **Qibing Zhan**,[1] **Xinjie Zhou**,[1] **and Mushuang Diao**[1]

[1]*State Key Laboratory of Plateau Ecology and Agriculture, School of Water Resources and Electric Power, Qinghai University, Xining, Qinghai Province 810016, China*
[2]*College of Architecture and Civil Engineering, Beijing University of Technology, Beijing 100124, China*
[3]*National Concrete Pavement Technology Center, Institute for Transportation, Ames, IA 50014, USA*

Correspondence should be addressed to Xinjian Sun; sunxj@qhu.edu.cn and Yifeng Ling; yling@iastate.edu

Received 23 April 2019; Revised 2 September 2019; Accepted 26 September 2019; Published 11 November 2019

Academic Editor: Luís C. Neves

This paper mainly investigates the fracture parameters of Basalt Fiber Reinforced Concrete (BFRC) with various fiber lengths and dosages using Double-K fracture model. The model was developed by fracture criterion using ABAQUS Virtual Crack Closure Technique (VCCT), and the results of the model and experiments were compared. The basalt fiber with length of 6 mm and 12 mm was added into concrete in the dosage of 0.0%, 0.1%, 0.2%, 0.3%, 0.4%, and 0.5% by volume of concrete, respectively. Concrete specimens were cast into three dimensions, i.e., 60 mm × 180 mm × 480 mm, 80 mm × 240 mm × 640 mm, and 100 mm × 300 mm × 800 mm. Then, three-point bending test was conducted on precast-notched beams. The load versus cracking mouth opening displacement (P-CMOD curve) was developed in order to evaluate cracking and breaking load. The initial fracture toughness and unstable fracture toughness were derived from the Double-K fracture model aimed to optimize the fiber length and dosage. The results showed that the initial fracture toughness and unstable fracture toughness increased first and then decreased with the increase in fiber dosage, and basalt fiber with length of 6 mm and dosage of 0.2% performed the best toughening effect on concrete. The comparison results showed that numerical simulation can better simulate the initiation and propagation of BFRC fractures and achieve the dynamic propagation process of fractures.

1. Introduction

The concrete panel rock-fill dam is extensively developed due to its low cost, short construction period, and strong adaptability, but concrete panel is vulnerable to cracks, which restricted its application. As a quasibrittle material, concrete has low tensile strength (tensile strength is 1/10 to 1/20 of compressive strength). In the process of casting, the concrete panel is in high risk to yield cracks due to uneven settlement, hydration reaction, and dry shrinkage deformation [1–3]. These cracks can cause seepage and remove fine particles in the panel, which seriously impacts the structural stability, reduces the antiseepage performance and durability of the concrete panel, and becomes a great threat to the safety of the dam [4–7].

According to previous research, adding fibers, such as steel fiber, carbon fiber, and polypropylene fiber into concrete, can improve the basic mechanical properties, ductility, toughness, crack resistance, and durability of concrete structures [8–10]. Steel fiber was a commonly used fiber type to enhance the basic mechanical properties of concrete. Pan et al. found that appropriate addition of steel fiber reduced the fragility of the concrete, improved the shape of the major crack, and increased the toughness and ductility of the concrete matrix [11–13]. However, addition of steel fiber raises the weight of concrete itself, which can result in

difficulty of construction and differential settlement in terms of mass concrete panels. Moreover, as a water retaining structure, concrete panel perennially contacts with water which makes steel fiber rust easily. Thus, it induces microcracks in the panel, causes the panel seepage, and further reduces its durability. Consequently, steel fiber is not suitable in concrete panel [14–16].

Carbon fiber has the advantages of high tensile strength, low density, large elastic modulus and strong toughness, so it was believed as a good fiber for improving concrete performance. Tong et al. put forward that proper amount of short-cut carbon fiber can enhance the tensile splitting strength, compressive strength, and flexural strength of concrete [17, 18]. Deng and Wang et al. studied the fracture parameters of carbon fiber concrete and concluded that carbon fiber could greatly improve the fracture energy, fracture toughness, and critical crack mouth opening displacement of concrete [19, 20]. However, carbon fiber is too expensive for a large amount of concrete panel pouring. Therefore, carbon fiber concrete has not been widely adopted in water conservancy construction.

Polypropylene fiber has been widely used in recent years. Liang et al. found that polypropylene fiber enhanced the bending performance of concrete and greatly improved the initiation toughness [21]. Nevertheless, the addition of polypropylene fiber declined the strength of concrete, and polypropylene fiber concrete was less effective in reducing dry shrinkage cracks [22]. It is not feasible for Qinghai area along with strong radiation and large temperature difference. Therefore, looking for a more suitable fiber to improve the crack resistance and durability of concrete in Qinghai province is necessary.

In recent years, both domestic and foreign scholars have found that basalt fiber can better improve the performance of concrete. Basalt fiber is formed by melting and drawing of basalt ore at high temperature. It has advantages such as high-temperature resistance, chemical resistance, good mechanical properties, and natural compatibility with concrete [23–27]. Research studies on BFRC have been carried out. Wang et al. found that basalt fiber could improve the splitting tensile and flexural strength of concrete, but it had a delayed effect on the early compressive strength of concrete [28]. Basalt fiber significantly enhanced the freeze-thaw resistance and durability of concrete under corrosion conditions [29]. Yu et al. claimed that basalt fiber was able to improve the impact resistance number and performance of BFRC [30]. Branston et al. pointed out that basalt fiber did not significantly improve the compressive strength and elastic modulus of high-strength concrete, but the tensile strength, ductility and crack resistance were improved [31]. High et al. addressed that basalt fiber had little effect on the compressive strength of concrete, but could enhance the flexural modulus [32]. According to Wang et al.'s study, at 0.2% basalt fiber dosage, no visible cracks were observed in concrete [33]. Xue et al. investigated the fracture parameters of BFRC using the calculation model provided by ASTM. Their results showed that, same as plain concrete, the fracture process of BFRC could also be divided into three stages, i.e., crack nonpropagation, crack stable propagation, and crack unstable propagation. Moreover, basalt fiber greatly improved the fracture parameters [34–36]. Wang et al. found that adding basalt fiber had effects on compressive strength, tensile splitting strength, flexural tensile strength and size effect, among which compressive strength had the greatest effect [37]. Based on previous studies, basalt fiber had great improvement on the durability and crack resistance of plain concrete.

Up to date, most of relevant research programs focused on the basic mechanical properties of BFRC. However, it is rarely employed to analyze fracture performance with Double-K fracture model. In this paper, the BFRC fracture parameters were analyzed by the Double-K fracture model. Double-K fracture model was put forward by Xu and Reinhardt, which described the fracture process of concrete by two stress intensity factors: initiation toughness and unstable fracture toughness. It introduced the unstable fracture toughness parameters and believed that the aggregate and mortar in concrete caused the increase of unstable fracture toughness. And the fracture of concrete could be divided into three stages: crack nonpropagation, crack stable propagation, and crack unstable propagation [34, 38–44]. Ruiz et al. investigated the effects of crack size and bond on Double-K fracture parameters of concrete [45]. The feasibility of using peak loads to determine Double-K parameters was demonstrated by Kumar et al. [46]. Wang et al. studied the Double-K fracture parameters of steel fiber reinforced concrete [47]. The Double-K fracture parameters of carbon fiber reinforced concrete were evaluated by Zhang et al. [48]. However, few researchers have applied Double-K fracture parameters to investigate the fracture performance of BFRC. Thus, it is significant to study the Double-K fracture parameters of BFRC.

For the constitutive model study of fracture, Bernardi et al. used nonlinear finite element on double-parameter simulation for polypropylene fiber concrete. Their results showed that the simulated results were highly coherent with the experimental results [49]. Chi et al. evaluated the value of damage constitutive model on steel and polypropylene fiber concrete by ABAQUS [50]. Hu et al. found that the deviations of the whole-process simulation on crack initiation, stable propagation, and unstable failure were less than 10% for three-point bending beam using extended finite element method (XFEM) [51]. Roth et al. utilized XFEM and distress to study concrete crack propagation [52]. Lu and Liu et al. studied the release rate of strain energy for composites using virtual crack closure technique (VCCT). The results indicated that the variations of the strain energy release rate from test and simulation were between 0.4% and 11.4% for type I and type II fracture, respectively [53]. Valvo accessed energy release rate of type I, II, and III compound cracks using VCCT [54]. The constitutive model has been widely studied in concrete materials, but VCCT has hardly been used to study the fracture behavior of BFRC. Comparing with XFEM, VCCT can better simulate the crack initiation and crack propagation of concrete and reduce time on calculations. Therefore, VCCT was selected to simulate and analyze fracture performance of BFRC.

2. Background

2.1. Double-K Fracture Parameters and Calculation. As a quasibrittle material, BFRC can be composed of base phase and dispersed phase. Base phase is a mixture of cement, water, fly ash, water-reducing agent, air entraining agent, and basalt fiber, while dispersed phase is the aggregate. The fracture failure of BFRC can be divided into three levels, the first level: the bonding surface of mortar and aggregate is a weak surface, and cracks are generated on the bonding surface of mortar and aggregate firstly; the second level: with the development of cracks between mortar and aggregate binding surfaces, cracks spread into mortar and the interface of sand and hardened cement slurry begins to crack; third level: as cracks between sand and hardened cement slurry develop, hardened cement slurry starts to crack, accompanied by the pulling-out failure of fibers. Xu and Reinhardt put forward the Double-K fracture model to evaluate the fracture properties of concrete more accurately. In Double-K fracture model, the fracture of concrete consists of three processes, namely, the nonpropagation crack, the stable-propagation crack, and the unstable-propagation crack. In order to better describe the fracture process, the initiation toughness (K_{IC}^{Q}) and unstable fracture toughness (K_{IC}^{S}) were introduced. When $K < K_{IC}^{Q}$, crack will not propagate; when $K_{IC}^{Q} = K$, crack starts stable propagation; when $K_{IC}^{Q} < K < K_{IC}^{S}$, crack is in stable propagation; and when $K_{IC}^{S} < K$, crack is in unstable propagation. In this paper, Double-K fracture parameters were determined according to P-CMOD curve.

2.2. Initiation Toughness. As a quasibrittle material, the crack propagation starts with linear elastic propagation, where crack has not yet appeared. Next stage is elastoplastic propagation, where the crack is stably propagating until the fracture load. Specimen is damaged in this stage. In P-CMOD curve, the load at turning point from the linear part to the nonlinear part is called the crack initiation load (F_Q). According to DL/T 5332-2005 [55], the initiation toughness can be expressed as

$$K_{IC}^{Q} = \frac{1.5 \times \left(F_Q + (mg/2) \times 10^{-2}\right) \times 10^{-3} \times S \times \sqrt{a_0}}{th^2} \times f(\alpha), \tag{1}$$

$$f(\alpha) = \frac{1.99 - \alpha(1-\alpha)\left(2.15 - 3.93\alpha + 2.7\alpha^2\right)}{(1+2\alpha)(1-\alpha)^{3/2}}, \tag{2}$$

where K_{IC}^{Q} is initiation toughness, MPa·m$^{1/2}$; F_Q is crack initiation load, kN; a_0 is length of precast crack, m; t is thickness of specimen, m; h is height of specimen, m; S is midspan distance, m; m is mass of midspan specimen, kg; and g is acceleration of gravity, 9.81 m/s^2.

2.3. Critical Effective Crack Length. The fracture process of BFRC specimen is not all linear due to the bond strength between aggregates and binder and the bridging effect of basalt fiber after matrix cracking. Therefore, the nonlinear characteristic is equivalent to elastic fracture when fracture occurs for calculation of unstable fracture toughness. Hereby, the critical effective crack length can be calculated following equation (3) as per DL/T 5332-2005 [55]:

$$a_c = \frac{2}{\pi}(h + h_0)\arctan\left(\frac{tEV_C}{32.6F_{max}} - 0.1135\right)^{1/2} - h_0, \tag{3}$$

where h_0 is the thickness of the edge sheet of the clip extensometer, m; V_C is the critical value of crack opening displacement, μm; and E is the elasticity (GPa) as expressed by

$$E = \frac{1}{tc_i}\left[3.70 + 32.60\tan^2\left(\frac{\pi}{2}\frac{a_0 + h_0}{h + h_0}\right)\right], \tag{4}$$

where a_0 is the length of precast crack, m, and c_i is the ratio of displacement to load in the linear stage of load displacement, μm/kN.

2.4. Unstable Fracture Toughness. When the load reaches the maximum, the specimen is in unstable state. The corresponding fracture toughness at this moment is the unstable fracture toughness. Based on DL/T 5332-2005 [55], unstable fracture toughness can be determined by equations (2) and (5):

$$K_{IC}^{Q} = \frac{1.5 \times \left(F_{max} + (mg/2) \times 10^{-2}\right) \times 10^{-3} \times S \times \sqrt{a_0}}{th^2} \times f(\alpha), \tag{5}$$

where K_{IC}^{S} is unstable fracture toughness, MPa·m$^{1/2}$; F_{max} is maximum load, kN; ac is critical effective crack length, m; t is thickness of specimen, m; h is height of specimen, m; S is midspan distance, m; m is mass of midspan specimen, kg; and g is acceleration of gravity, 9.81 m/s^2.

In this paper, three-point bending tests were carried out for precast notched BFRC beams with different lengths, admixtures, and specimen sizes. The load versus cracking mouth opening displacement curves (P-CMOD curves) were developed in order to evaluate cracking and fracture load. The initiation toughness and unstable toughness parameters of BFRC were calculated by using the Double-K fracture model. The effects of basalt fiber length and content on fracture properties of BFRC were analyzed as well. Due to the limited test conditions, the entire process of BFRC fracture is difficult to determine. Therefore, VCCT technique was used to simulate the fracture performance of BFRC and analyze the entire process of BFRC fracture.

3. Experimental Work

3.1. Materials. The properties of used ordinary Portland cement were tested according to GB/T 17671-1999 [56], GB/T 1346-2011 [57], GB/T 1345-2005 [58], and GB175-2007 [59], as shown in Table 1.

II grade fly ash was used in this paper, and its properties are listed in Table 2 as per DL/T 5055-2007 [60].

Table 1: Properties of Portland cement.

Test	Cement type	Strength grade	Rupture strength (MPa)		Compressive strength (MPa)		Setting time (min)		Standard consistency (%)	Soundness (mm)
			3 d	28 d	3 d	28 d	Initial setting	Final setting		
Result	P.O	42.5	5.20	7.8	20.1	45.2	155	255	28.0	1.5
Specification	P.O	42.5	≥3.5	≥6.5	≥17.0	≥42.5	≥45	≤600	—	≤5.0

Table 2: Properties of fly ash.

Test	Fineness (45 μm) (%)	Water demand ratio (%)	Ignition loss (%)	Moisture content (%)	Stability (mm)
Result	14.7	96	2.6	0.2	1.5
Specification/II	≤25	≤105	≤8	≤1.0	≤5.0

The properties of used water-reducing admixture and air entraining admixture are shown in Tables 3 and 4 based on DL/T 5100-2014 [61].

Coarse aggregate and fine aggregate are natural aggregates (containing artificial crushed pebbles) from the right bank of Yangqu Hydropower Station. Their properties are summarized in Tables 5 and 6 according to DL/T 5144-2015 [62] and DL/T 5151-2014 [63].

The properties of basalt fibers used in the test are shown in Table 7, and the samples are shown in Figure 1.

The proportion of BFRC is presented in Table 8 according to JGJ/T 22l-2010 [64] and DL/T 5330-2015 [65].

3.2. Specimen Preparation. In this study, a forced mixer was used to mix BFRC. Coarse aggregate and fine aggregate were mixed for 30 s first. In order to ensure a uniform distribution of the basalt fibers in concrete, a dry fiber mixing method was used to improve the uniformity of fiber distribution based on [66]. Cement, fly ash, and superplasticizers were poured to mix for another 30 s. Then, basalt fibers were spread uniformly into mixer followed by 60 s mixing. After water and AEA adding, all materials were mixed for 60 s at last. Next, the mixed BFRC was cast and then consolidated using a table vibrator, followed by surface finishing. After 24 h, specimens were demolded and cured in standard curing room for 28 days. Before three-point bending test, specimens were cut to preform crack as required using cutting machine. In order to avoid error caused during specimen preparation, all specimens were prepared once.

Three different dimensions of specimens used for three-point bending test were 60 mm × 180 mm × 480.6 mm, 80 mm × 240 mm × 640.8 mm, and 100 mm × 300 mm × 801 mm, respectively. Basalt fibers of 6 mm length were added to the mixture in accordance with the dosage of 0%, 0.1%, 0.2%, 0.3%, 0.4%, and 0.5%, respectively, the same for the basalt fiber of 12 mm length. The detailed information of specimens is listed in Table 9.

3.3. Test Equipment. Three-point bending test was carried out at continuous loading rate of 0.4 MPa/min using Kaiwen universal hydraulic machine. A linear variable differential transformer (LVDT) sensor was installed vertically at the bottom of beam two centimeters from the midspan to measure vertical displacement. An extensometer was mounted at precast crack incision to determine CMOD. Resistance strain gauges (model: S2150-150AA, resistance: 149.5 ± 0.2%, sensitivity coefficient: 2.032 ± 0.32%, grid width: 5 mm, grid length: 150 mm) were pasted every 2 cm at the top of the precast crack. The specimen under loading is illustrated in Figure 2.

4. Experiment Results and Discussion

4.1. P-CMOD Curves. The effects of various basalt fiber dosage on P-CMOD curve were obtained from the tests as shown in Figures 3 and 4 for 6 mm fiber and 12 mm fiber, respectively.

According to the P-CMOD curve analysis, in general, the expansion of concrete cracks can be divided into three stages (stage I, stage II, and stage III). Stage I: at the beginning of load application, the load and displacement were in linear relationship. At this moment, BFRC had not started to crack. In this stage, BFRC elastically expanded. Stage II: with load continuing, the microcracks occurred under steady propagation until the ultimate load was reached. BFRC displayed a nonlinear expansion, with the growth of microcracks. It stepped into matrix fracture Stage III: After ultimate load, unstable fracture took over in crack propagation until the cracks produced over the whole specimen. In this stage, the specimen was completely fractured along with the fibers pulling out. In this test, the fracture process of most tested specimens was exhibited these three stages, while some type A and B specimens only had stage I and stage III. The nonlinear rising stage is not apparent enough. This might be due two reasons: (1) the yield process is relatively short and lose a lot of yield values during force load; (2) the sizes of type A and B specimens are relatively small, and the existed size effect leads to small yield strength for type A and B specimens and the relatively short yield process. In the future tests, displacement loading should be selected to better collect BFRC fracture data and analyze BFRC fracture

Table 3: Properties of water-reducing admixture.

Test	Dosage (%)	Water educing rate (%)	Air content (%)	Ratio of bleeding rate (%)	Setting time difference (min)		Compressive strength ratio 9%)		
					Initial setting	Final setting	3 d	7 d	28 d
Result	1.0	17.0	1.3	82	28	32	141	138	129
Specification	0.8~1.2	≥15	<3.0	≤90	−60~+90	−60~+90	≥130	≥125	≥120

Table 4: Properties of air entraining admixture.

Test	Dosage (%)	Water reducing rate (%)	Air content (%)	Ratio of bleeding rate (%)	1 h change in air content (mm)	Setting time difference (min)		Compressive strength ratio (%)		
						Initial setting	Final setting	3 d	7 d	28 d
Result	0.04	6.0	5.2	53	1.2	35	26	116	102	96
Specification	0.02~0.05	≥6	4.5~5.5	≤70	−1.5~+1.5	−90~+120	−90~+120	≥90	≥90	≥85

Table 5: Fine aggregate particle gradation.

Aggregate size (mm)	4.75	2.36	1.18	0.60	0.300	0.15	≤0.15
Accumulated sieve residue (%)	2.5	27.3	45.3	60.7	82.4	93.5	99.6

Table 6: Coarse aggregate particle gradation.

Aggregate size (mm)	2.36	4.75	9.5	16	19	26	31.5	37.5
Accumulated sieve residue (%)	100	98.9	82.4	54.6	50.2	33.9	11.8	0

Table 7: Properties of basalt fibers.

Length (mm)	Diameter (μm)	Tensile strength (MPa)	Elasticity (GPa)	Elongation (%)	Density (kg/m^3)
6/12	17.4	≥2000	≥85	2.5	2699

performance. For a given specimen size, the incorporation of basalt fiber improved the ultimate load and CMOD of concrete because the high tensile strength of basalt fiber inhibited the crack propagation of concrete during pull-out process of fibers.

4.2. Double-K Fracture Parameters Calculation and Discussion

4.2.1. Double-K Fracture Parameters Calculation. Using the Double-K fracture model, the BFRC fracture parameters were calculated according to the measured load, displacement, and their corresponding parameters, as shown in Table 10.

According to Table 10, the initiation toughness and unstable toughness showed irregular growth. However, compared with PC, the growth rates of the initiation toughness and unstable toughness are 1.023–1.736 and 1.015–1.541, respectively. Because concrete will shrink during the forming process, the shrinkage will cause relative displacement of the concrete matrix. The scattered distribution of basalt fibers could prevent the movement of the matrix aggregate and withstand the tensile stress caused by shrinkage, reducing the stress concentration, preventing the expansion of the crack, and enhancing the fracture toughness of concrete. In the process of fracture failure of basalt fiber concrete, the fiber will be pulled out from the matrix, prolonging the stable expansion stage of the basalt fiber concrete specimen and enhancing the fracture toughness of the concrete.

4.2.2. Initiation Toughness Discussion. BFRC fracture propagation is a complex process. The defects such as microcracks, voids, and weak contact surface between mortar and aggregates exist in BFRC matrix among which most of them are interfacial cracks and very few are mortar cracks. At the beginning of loading, it exhibits the elastic stage because these defects are stable. In the process of increasing the load until it reaches the critical load, these microcracks, voids, and weak surfaces between mortar and aggregate begin to extend or expand, which shows the linear stage for BFRC fracture. The development process of these defects depends on the magnitude of the crack initiation load and initiation toughness. Thus, crack initiation load and initiation toughness play an important role in evaluating crack resistance of concrete materials.

Figure 4 shows that with the increase in dosage for 6 mm long basalt fiber from 0.0% to 0.5%, the initiation toughness

(a) (b)

Figure 1: Basalt fiber of different lengths. (a) 6 mm basalt fibers. (b) 12 mm basalt fibers.

Table 8: BFRC proportion (kg).

Fly ash	Cement	Water	Sand	Small stone	Medium stone	AEA	Superplasticizer
57	226	130	688	638	638	1.13	2.83

Table 9: Detailed information of specimens.

Specimen	Dimension (mm)	Span length (mm)	Span-depth ratio	Precast crack length (mm)	Seam height ratio
A	$60 \times 180 \times 480$	450	2.5	36	0.2
B	$80 \times 240 \times 640$	600	2.5	48	0.2
C	$100 \times 300 \times 800$	750	2.5	60	0.2

Note. All specimens are not listed here due to tremendous quantity. The specimen is identified by *X*-*Y*-*Z*, where *X* represents size of specimen, *Y* is length of basalt fiber, and *Z* stands for fiber content. A is the specimen in dimension of 60 mm × 180 mm × 480 mm, B is the specimen in dimension of 80 mm × 240 mm × 640 mm, and C is the specimen in dimension of 100 mm × 300 mm × 800 mm.

increased first and decreased after 0.2% dosage. The initiation toughness of BFRC was greater than that of plain concrete. Regardless of specimen dimension, initiation toughness was maximum at 0.2% dosage. However, initiation toughness of specimens A increased most which is up to 61.55%. When the basalt fiber content was 0.4%, the initiation toughness was relatively small. The reason might be that the fiber agglomeration caused defects such as microcracks and voids in the concrete.

As the raise of dosage for 12 mm long basalt fiber, initiation toughness increased first and then decreased as well. Compared with the plain concrete, the addition of basalt fiber increased initiation toughness. For different dimensions of specimen, the maximum initiation toughness appeared at different fiber dosage. For instance, the peak values of initiation toughness for A and B specimens are at 0.2% fiber dosage, but it was 0.3% for C specimens. The initiation toughness of A specimens was improved most up to 73.6% among the three dimensions of specimen.

Generally, considering the time of crack development, the optimal dosage of basalt fiber was 0.2%. Regarding the increment of initiation toughness, the BFRC with 6 mm basalt fiber displayed relatively stable increase in initiation toughness. Among the BFRC specimens with 12 mm basalt fiber, only one specimen performed a large raise in initiation toughness probably due to randomness. Overall, the optimal combination of basalt fiber was 6 mm in length and 0.2% in dosage. Basalt fiber could increase the initiation toughness because it had higher strength and ductility than the plain concrete. Basalt fibers scattered and connected with each other in concrete matrix, which could inhibit the development of microcracks, voids, and the weak interface of mortar and aggregate, prolong the linear propagation and increase the initiation toughness. However, it should be noted that if the basalt fibers are distributed inhomogeneously and clustered together, they cannot well restrain the development of microcracks, voids, and weak interface in concrete and even lead to the decline of initiation toughness. This is associated with the voids among the fibers and the very low friction among the fibers.

4.2.3. Unstable Fracture Toughness Discussion. After linear propagation, BFRC started unstable failure until it reached the ultimate load and failed. Figure 5 presents the trends of unstable fracture toughness with various basalt fiber dosages.

As the load increases, the crack in BFRC ends linear stage and steps into the nonlinear stage. In this stage, the

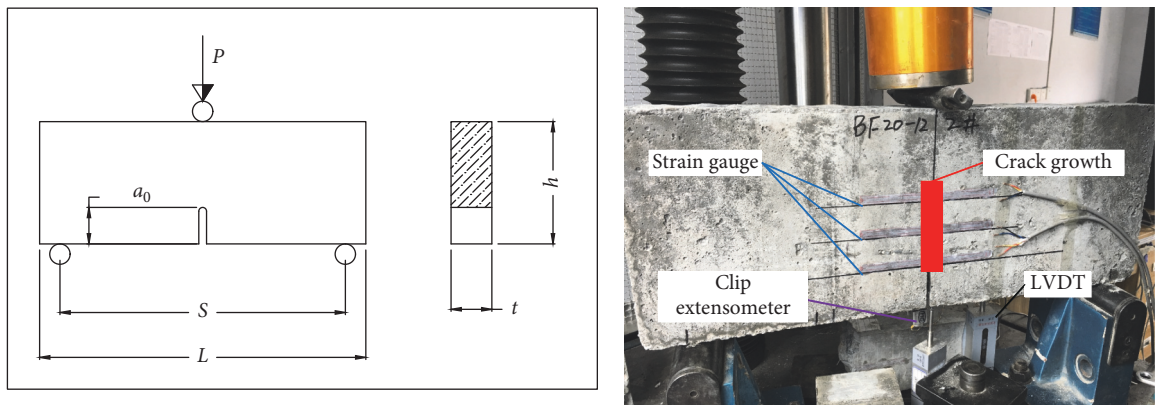

(a) (b)

Figure 2: Three-point bending test. (a) Loading diagram. (b) Under test. Note: P is the applied load, L is length of specimen, h is height of specimen, t is thickness of specimen, S is span interval, and a_0 is height of prefabricated crack.

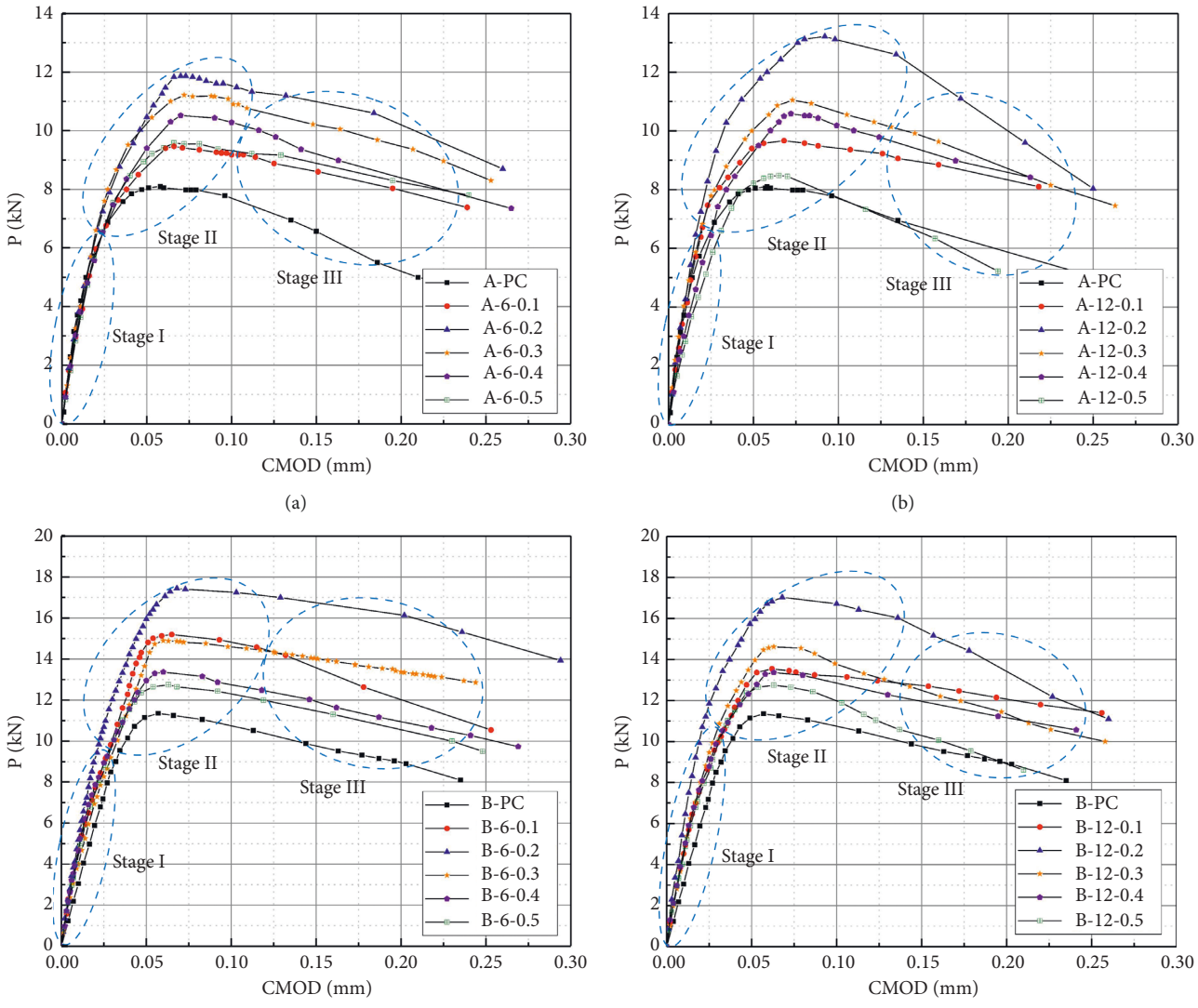

Figure 3: Continued.

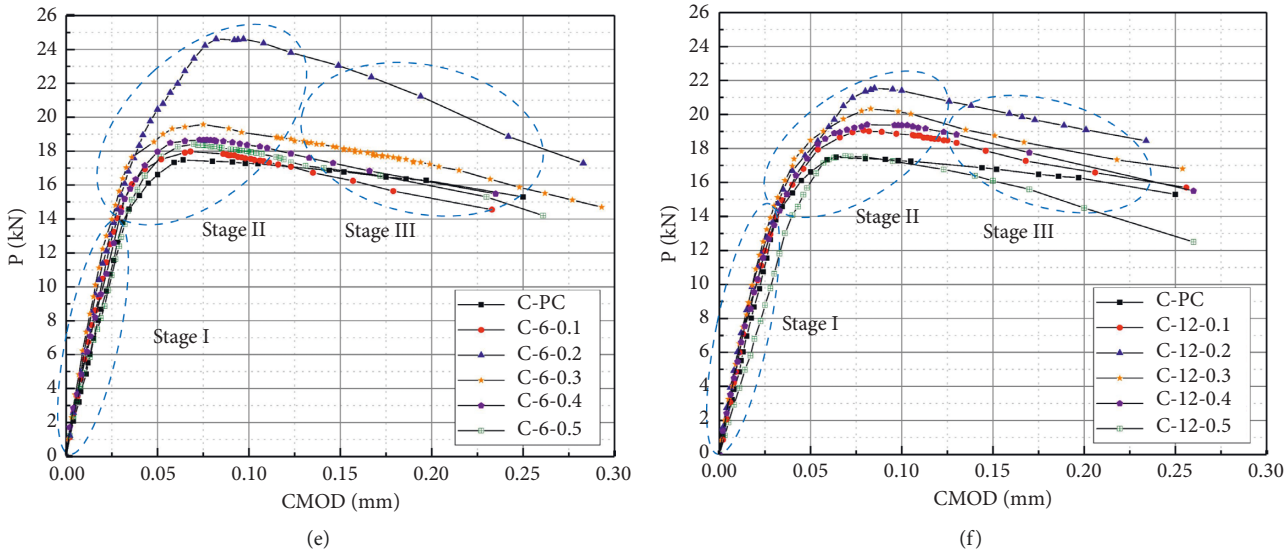

Figure 3: P-CMOD curves for 6 mm and 12 mm basalt fiber with various dosages. (a) Specimen A and fiber length 6 mm. (b) Specimen A and fiber length 12 mm. (c) Specimen B and fiber length 6 mm. (d) Specimen B and fiber length 12 mm. (e) Specimen C and fiber length 6 mm. (f) Specimen C and fiber length 12 mm.

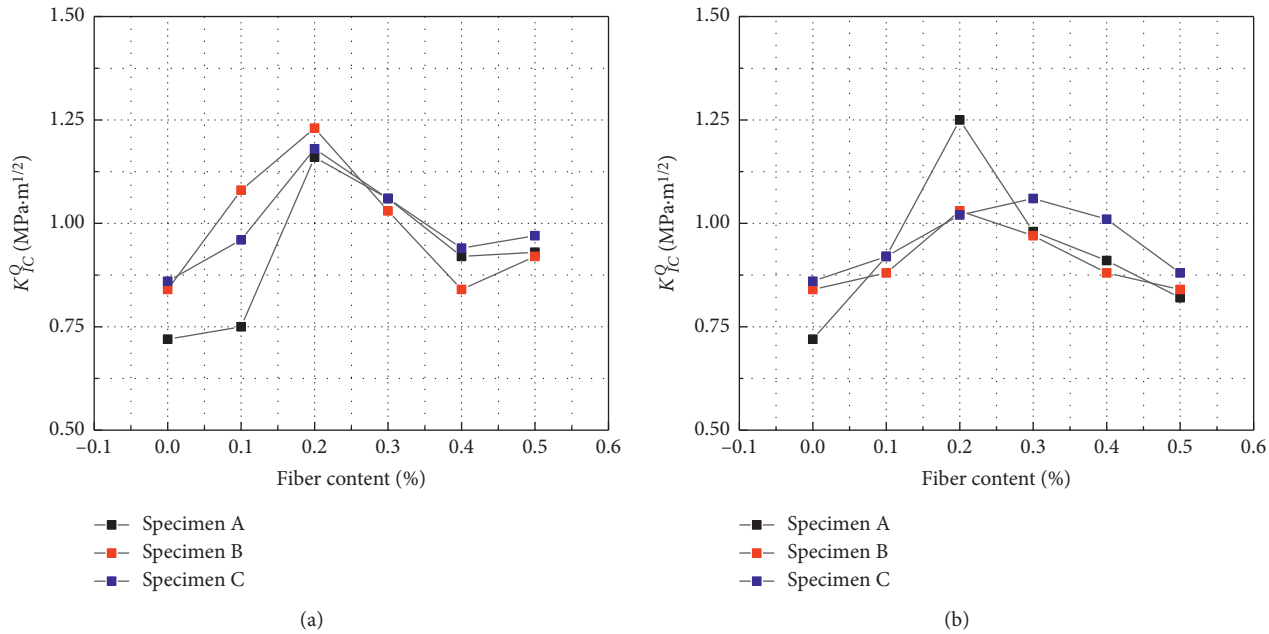

Figure 4: Initiation toughness vs. basalt fiber dosage. (a) The fiber length is 6 mm. (b) The fiber length is 12 mm.

defects such as the microcracks, voids, and weak contact surface between substrate and aggregate continue to develop. Cracks and other defects occurred in the mortar, meanwhile sand and interface of hardened cement slurry were damaged, resulting in crack propagation into the slurry. When the slurry damaged, the specimen failed. The fracture failure limit of BFRC depends upon the unstable load and unstable fracture toughness, which plays an important role in the evaluation of fracture performance.

Based on Figure 5, similar trends of unstable fracture toughness for both 6 mm and 12 mm fibers can be obtained comparing with Figure 5. It can be observed that the maximum unstable fracture toughness was at 0.3% fiber dosage for A specimens and at 0.2% for B, C specimens when introducing 6 mm fibers. While for the specimens with 12 mm fibers, the peak value of unstable fracture toughness was achieved at 0.2% fiber dosage for A, B specimens and at 0.3% for C specimens. Specimens of A dimension had the most increment up to 62.5% at 0.2% dosage.

Table 10: BFRC fracture parameters with various basalt fiber content and dosage.

Group	Specimen ID	P_{ini} (kN)	$CMOD_{ini}$ (μm)	P_{max} (kN)	$CMOD_{max}$ (μm)	E (GPa)	a_c (μm)	K_{Ic}^{ini} (MPa · m$^{1/2}$)	K_{Ic}^{un} E(MPa · m$^{1/2}$)
A	A-PC	5.73	18	8.1	58	39.66	64	0.72	1.48
	A-6-0.1	5.97	20	9.47	66	37.14	61	0.75	1.64
	A-6-0.2	9.57	42	12.35	76	28.36	46	1.16	1.75
	A-6-0.3	8.67	32	11.22	72	33.72	55	1.06	1.77
	A-6-0.4	7.47	30	10.52	70	30.99	53	0.92	1.63
	A-6-0.5	7.55	30	9.58	66	31.33	55	0.93	1.52
	A-PC	5.73	18	8.1	58	39.66	64	0.72	1.48
	A12-0.1	7.47	23	9.67	68	40.42	64	0.92	1.76
	A12-0.2	10.28	34	13.22	92	37.66	61	1.25	2.28
	A12-0.3	7.98	27	11.05	73	36.81	59	0.98	1.85
	A12-0.4	7.42	29	10.58	72	31.84	55	0.91	1.68
	A12-0.5	6.60	31	8.48	65	26.51	53	0.82	1.32
B	B-PC	8.5	29	11.35	57	32.06	73	0.84	1.23
	B-6-0.1	13.28	42	15.20	65	29.20	62	1.08	1.42
	B-6-0.2	15.28	46	17.45	68	30.68	60	1.23	1.59
	B-6-0.3	12.53	44	14.89	60	26.30	54	1.03	1.29
	B-6-0.4	10.05	31	13.37	60	29.93	65	0.84	1.31
	B-6-0.5	11.07	36	12.75	63	28.38	67	0.92	1.28
	B-PC	8.5	29	11.35	57	32.06	73	0.84	1.23
	B-12-0.1	10.60	34	13.40	72	28.78	71	0.88	1.40
	B-12-0.2	12.60	29	17.03	68	40.11	73	1.03	1.78
	B-12-0.3	11.73	36	14.62	63	30.09	64	0.97	1.40
	B-12-0.4	10.53	33	13.37	63	29.47	67	0.88	1.33
	B-12-0.5	10.07	31	12.75	63	29.98	70	0.84	1.32
C	C-PC	13.8	31	17.48	64	32.66	88	0.86	1.35
	C-6-0.1	14.65	30	17.98	68	35.82	95	0.91	1.47
	C-6-0.2	19.77	46	24.62	82	31.52	80	1.18	1.72
	C-6-0.3	17.63	36	19.57	75	35.93	96	1.06	1.59
	C-6-0.4	15.18	32	18.67	73	34.81	95	0.94	1.52
	C-6-0.5	15.78	39	18.42	70	29.69	85	0.97	1.37
	C-PC	13.8	31	17.48	64	32.66	88	0.86	1.35
	C-12-0.1	14.95	34.5	19.07	79	31.79	93	0.92	1.52
	C-12-0.2	16.68	40	21.55	85	30.60	88	1.02	1.63
	C-12-0.3	17.38	41	20.17	92	31.10	97	1.06	1.66
	C-12-0.4	16.42	42	19.40	81	28.67	88	1.01	1.48
	C-12-0.5	14.08	40	17.57	69	25.83	79	0.88	1.25

According to Figure 5, the optimal content of basalt fiber is 0.2% for 12 mm considering the failure of the specimen. However, the long fiber will wrap a large amount of water during mixing process, which will adversely affect slump of concrete and construction. Therefore, 6 mm basalt fiber is recommended in practical project. Basalt fiber can increase unstable fracture toughness of concrete. Its mechanism is that basalt fiber can be scattered in the concrete, connecting with each other. When crack propagates to cement slurry and cement damages, accompanied by tensile failure of basalt fiber (>2000 MPa), basalt fiber delays the crack propagation and the slurry destruction owing to large consumption of energy during crack propagation which explains that the fracture process of BFRC presents a certain plastic zone.

5. Numerical Simulation and Analysis

BFRC is a quasibrittle material with complex fracture mechanism. The three-point bending fracture test in the laboratory is difficult to keep tracking the fracture behaviors during the loading process beyond the ultimate load. With the development of computer technology, the macromechanical properties can be characterized using mesh division, finite element calculation, and fracture behavior simulation for concrete. It is very helpful to access fracture performance of BFRC under the correct numerical simulation by ABAQUS, a commercial software, which was used for the finite element modeling. Virtual crack closure technique (VCCT) was first proposed by Rybicki and Kanninen when they studied linear crack problems [67]. Shivakumar et al. applied VCCT to investigate surface crack of concrete [68]. The accuracy and applicability of VCCT in nonlinear materials have been verified by Cao et al. [69]. Additionally, in finite element analysis, VCCT is almost unaffected by mesh size in the calculation process, and shorten the finite element analysis steps, which greatly improves the calculation efficiency [70]. Therefore, VCCT was used to numerically simulate the fracture performance of basalt fiber reinforce concrete.

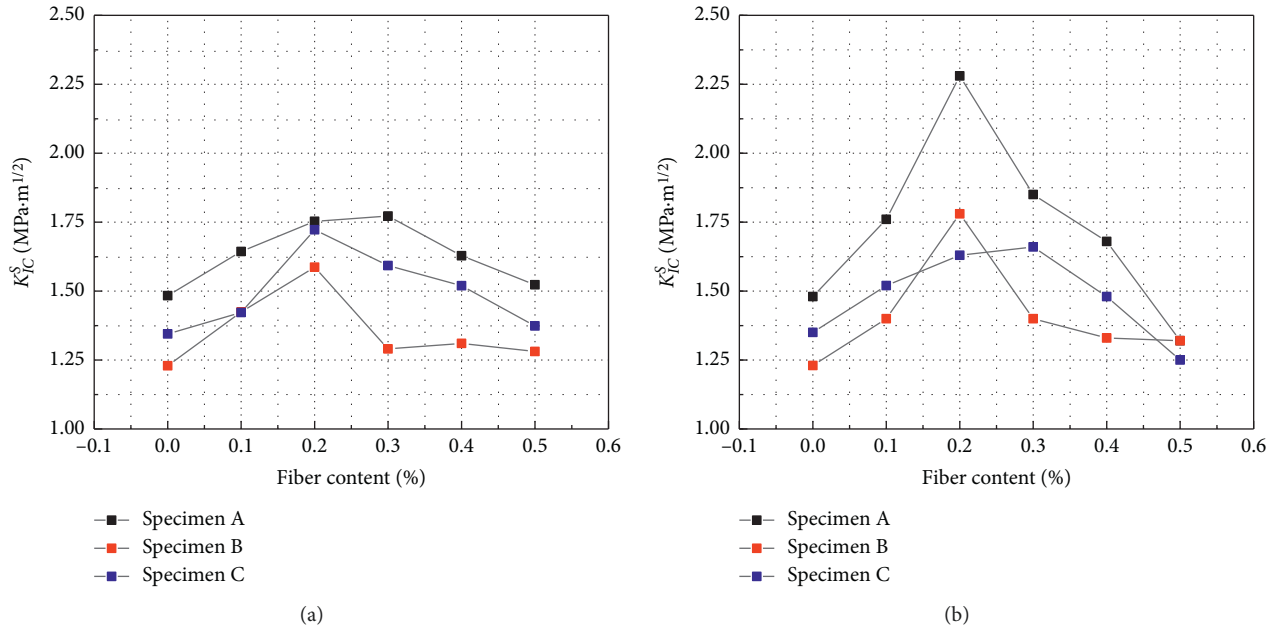

Figure 5: Unstable fracture toughness vs. basalt fiber dosage. (a) The fiber length is 6 mm. (b) The fiber length is 12 mm.

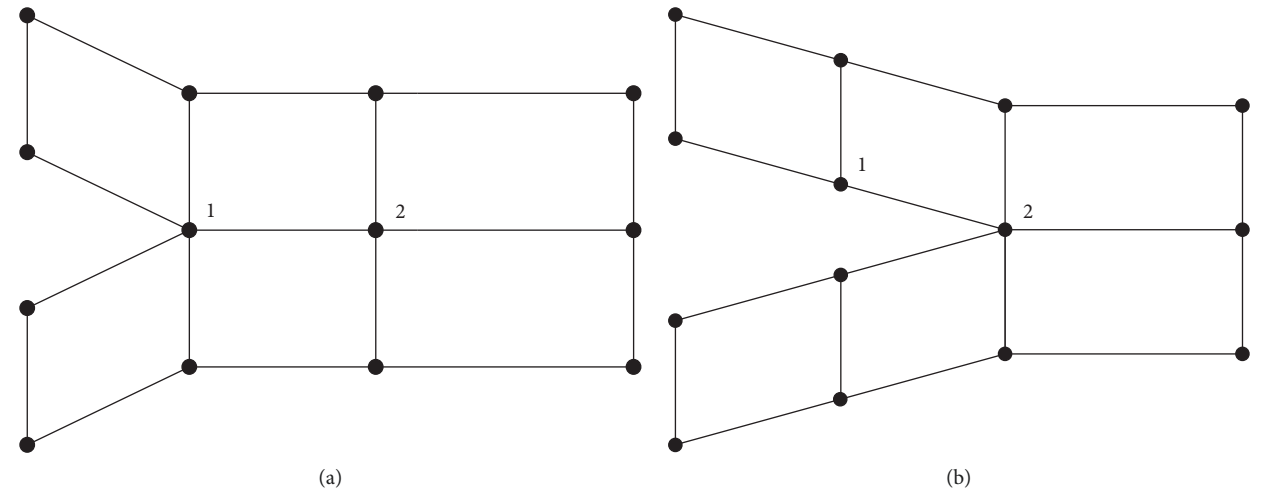

Figure 6: Process of crack propagation. (a) Before crack propagation. (b) After crack propagation.

5.1. Virtual Crack Closure Technique (VCCT). VCCT is based on Irwin energy theory, and its core idea is to assume that the energy released from crack propagation equates to the energy for crack closure.

When the crack develops from Figure 6(a) to 6(b), assuming the front shape of the crack is constant, the opening size of the crack after propagation is the same as before. During crack propagation, assume that the energy release rate is G_I, and the critical energy release rate required for crack propagation is G_{IC}. When $G_I > G_{IC}$, crack propagates. Equation (6) can be used to assess if crack starts to initiates:

$$f = \frac{G_I}{G_{IC}} = \frac{1}{2}\left(\frac{v_{1.2}F_{v,3,4}}{b\,d}\right)\frac{1}{G_{IC}} \geq 1. \quad (6)$$

If $f > 1$, crack starts to propagate, where b and d represent the width and length of the unit crack tip. As shown in Figure 7, $F_{V,3,4}$ is the normal force between nodes 3 and 4; $v_{1,2}$ represents the normal displacement between nodes 1 and 2.

However, this rule of propagation is only suitable for type I fracture. The equivalent strain energy release rate G_e has to be introduced. Then, the criterion of crack propagation is $f = (G_e/G_{eC}) \geq 1$. ABAQUS provides BK criterion, POWER criterion, and Reeder criterion to calculate G_e.

BK criterion is the best criterion in this case that critical strain energy release rates on two shear directions are the same. Therefore, BK criterion was adopted in the simulation as shown in the following equation:

$$G_{eC} = G_{IC} + (G_{IIC} - G_{IC})\left(\frac{G_{II} + G_{III}}{G_I + G_{II} + G_{III}}\right)\eta, \quad (7)$$

where G_{eC} is equivalent strain energy release rate; G_I, G_{II}, and G_{III} are crack strain energy release rates of type I, II, and III

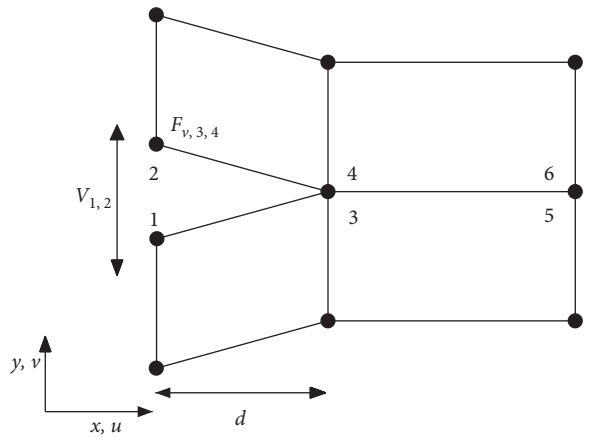

Figure 7: Crack propagation diagram.

Table 11: BFRC model parameters.

Specimen ID	Density	Elastic modulus	Poisson's ratio	Crack initiation energy release rate	Fracture energy release rate	η
A-6-0.2	2.38×10^{-9}	3.00×10^{4}	0.190	0.034	0.054	1.75
B-6-0.2	2.38×10^{-9}	3.07×10^{4}	0.200	0.035	0.048	1.75
C-6-0.2	2.38×10^{-9}	3.15×10^{4}	0.200	0.037	0.054	1.75
A-12-0.2	2.38×10^{-9}	3.03×10^{4}	0.193	0.040	0.072	1.75
B-12-0.2	2.38×10^{-9}	3.00×10^{4}	0.190	0.030	0.060	1.75
C-12-0.2	2.38×10^{-9}	3.14×10^{4}	0.205	0..032	0.052	1.75

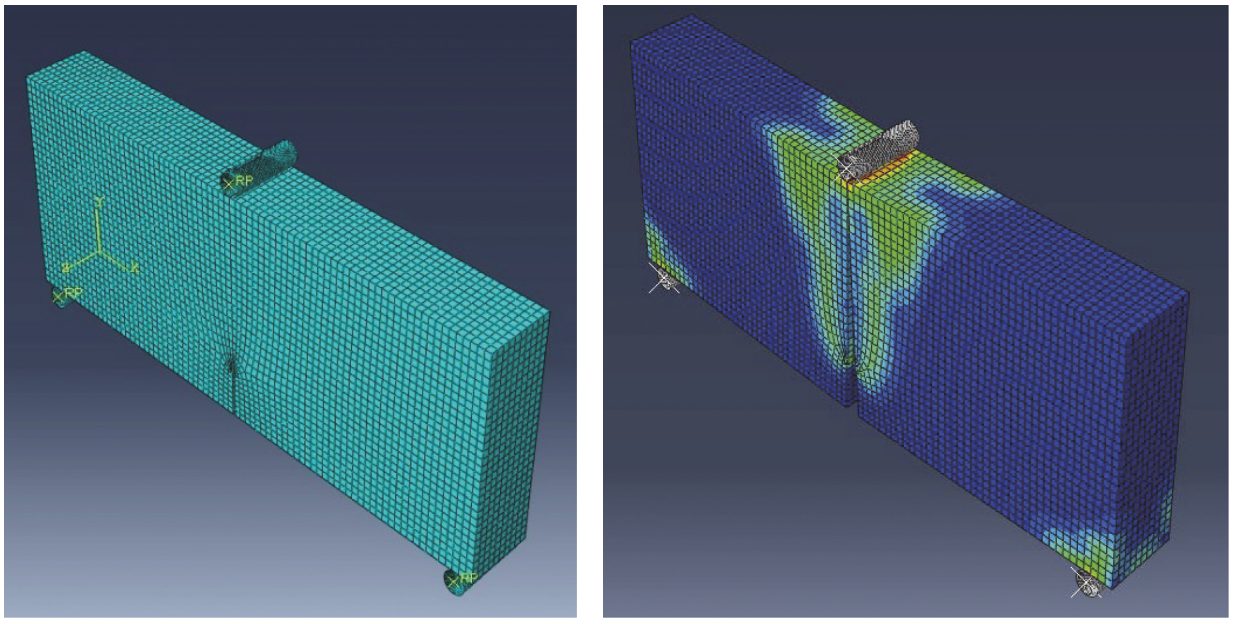

(a) (b)

Figure 8: Numerical analysis of mesh division and stress map. (a) Mesh division. (b) Stress pattern.

crack, respectively; and G_{IC}, G_{IIC}, and G_{IIIC} are critical crack strain energy release rates of type I, II, and III crack, respectively. η is usually between 0.5 and 2.5 for damage factor.

5.2. Comparison between Experimental and Numerical Results. The finite element method was used to simulate the experiment in ABAQUS software. Units are mm, N, tonne, MPa, tonne/mm^3, and MPa·mm$^{1/2}$. Hexahedral mesh was selected. The dimension of model and experiment was exactly the same. In order to better simulate the BFRC fracture process, enhanced VCCT was selected because it can simulate the crack initiation, which is more consistent with the real process. The parameters used in this simulation include

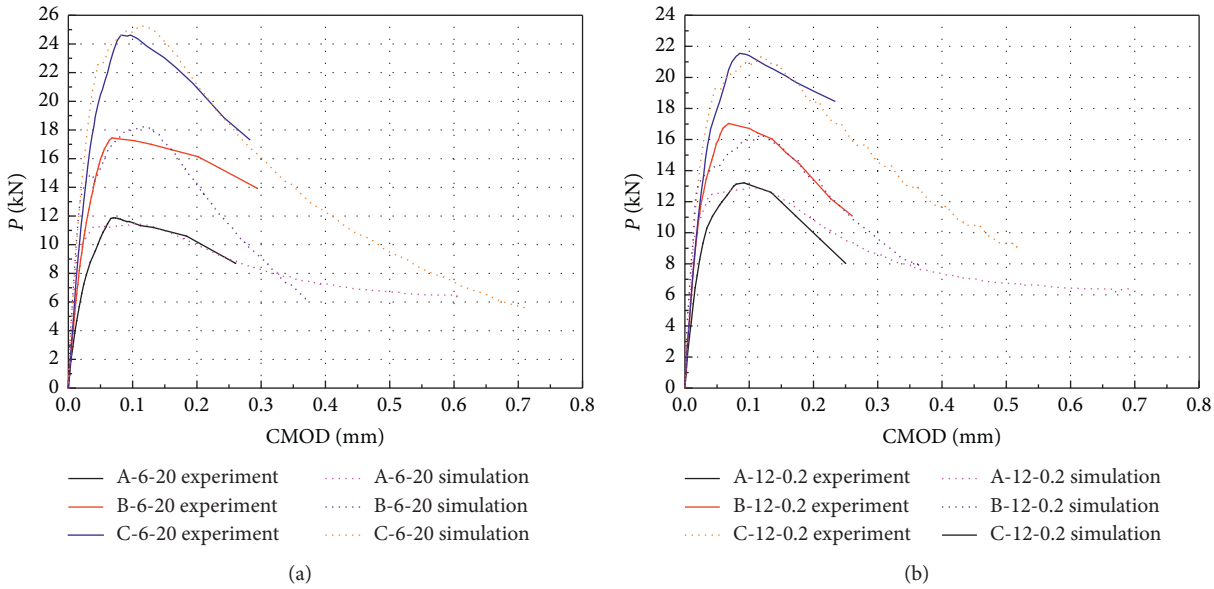

Figure 9: Comparison of results from numerical simulations and experiments. (a) 6 mm BFRC. (b) 12 mm BFRC.

density, elastic modulus, Poisson's ratio, crack initiation energy release rate, fracture energy release rate, and damage factor η. The density was measured by the experiments, and the elastic modulus, the crack initiation energy release rate, and the fracture energy release rate were calculated according to the DL/T5332-2005 [55]. Poisson's ratio was obtained based on the GB 50010-2010 [71]. The damage factor η is 1.75 according to empirical research. The specific parameters are shown in Table 11.

The mesh division and stress pattern are shown in Figure 9.

It can be seen from Figure 8 that the cracks initiated using VCCT to simulate the three-point bending and the stress were completely symmetrical, which is coherent with the real condition, and stress is concentrated in the three supports. The anticipated result was relatively acceptable as well. The three-point bending test on the specimens with 0.2% dosage of basalt fiber in 6 and 12 mm was selected to be simulated. The comparison results from simulation and experiments are presented in Figure 9.

Based on Figure 9, it indicates that under loading, the curves first rise linearly and then go up nonlinearly until reaching the peak value. The softening phenomenon occurred at some point in the descending stage. Regarding the coherence of the results from experiments and numerical simulation, it is relatively high before the peak value but it becomes low for B-6-20 after peak value. Nevertheless, the length of crack can be obtained up to 0.7 mm for numerical simulation but only about 0.4 mm for experiments. The agreement of critical displacement is not good due to displacement load. In other words, the loading rate is relatively high for displacement load. It is difficult to collect data after peak value.

6. Conclusion

In this paper, three-point bending tests were conducted on BFRC with two lengths (6 mm and 12 mm) and five dosages (0.1%, 0.2%, 0.3%, 0.4%, and 0.5%) and plain concrete as well. The optimum dosage of basalt fiber, initiation toughness, and unstable fracture toughness were evaluated. The conclusions are as follows:

(1) Basalt fiber can enhance the initiation toughness and unstable fracture toughness of concrete. Moreover, it can be uniformly distributed in the concrete matrix, preventing the development of microcracks, voids, weak interface due to basalt fiber bridging effect and enhancing the crack resistance of concrete.

(2) The P-CMOD curves were established by experiments, and the initial crack load was obtained based on the state of crack propagation. The initiation toughness was calculated by initial crack load. Basalt fiber increased initiation toughness. The optimal dosage of basalt fiber was 0.2%, and the toughening effect of 6 mm basalt fiber was better than that of 12 mm basalt fiber. Meanwhile, the slump of BFRC was also good to meet the requirement of engineering construction.

(3) Based on P-CMOD curves, when the load reached the maximum, the specimens failure. The buckling load and unstable fracture toughness were determined. Basalt fiber enhanced unstable fracture toughness. The optimal dosage of basalt fiber was 0.2%, while the toughening effect of 12 mm basalt fiber was better compared to 6 mm basalt fiber.

(4) The results of three-point bending test for the BFRC were analyzed using VCCT. The overall trend from numerical simulation results and the experiment results showed a high degree in coherence. Numerical simulation can better present the whole process of BFRC fracture. However, the numerical simulation and experimental results have some errors in the critical displacement fitting.

Data Availability

The data used to support the findings of this study are available from the corresponding author upon request.

Conflicts of Interest

The authors declare that they have no conflicts of interest.

Acknowledgments

This work was financially supported by the National Natural Science Foundation of China (Grant no. 51969026) and the Natural Science Foundation of Qinghai Province in China (Grant nos. 2017-ZJ-933Q and 2018-ZJ-750).

References

[1] R. Combrinck, L. Steyl, and W. P. Boshoff, "Interaction between settlement and shrinkage cracking in plastic concrete," *Construction and Building Materials*, vol. 185, pp. 1–11, 2018.

[2] V. A. Perfilov, D. V. Oreshkin, and D. Y. Zemlyanushnov, "Concrete strength and crack resistance control," *Procedia Engineering*, vol. 150, pp. 1474–1478, 2016.

[3] P. Cao, G. D. Li, J. J. Yu, M. Zhang, F. Jin, and M. Zhao, "Research and application of random aggregate model in determining the fracture behavior of four-point bending beam with notch," *Construction and Building Materials*, vol. 202, pp. 276–289, 2019.

[4] Z. Wang, S. Liu, L. Vallejo, and L. Wang, "Numerical analysis of the causes of face slab cracks in Gongboxia rockfill dam," *Engineering Geology*, vol. 181, pp. 224–232, 2014.

[5] M. Ahmed, J. Mallick, and M. Abul Hasan, "A study of factors affecting the flexural tensile strength of concrete," *Journal of King Saud University—Engineering Sciences*, vol. 28, no. 2, pp. 147–156, 2016.

[6] N. H. Li and Z. Y. Yang, "Technical progress of concrete face rockfill dam in China," *Chinese Journal of Geotechnical Engineering*, vol. 34, no. 8, pp. 1361–1368, 2012.

[7] H. Ma and F. Chi, "Technical progress on researches for the safety of high concrete-faced rockfill dams," *Engineering*, vol. 2, no. 3, pp. 332–339, 2016.

[8] K. Krayushkina, T. Khymerik, O. Skrypchenko, I. Moshkovskyi, and V. Pershakov, "Investigation of fiber concrete for road and bridge building," *Procedia Engineering*, vol. 187, pp. 620–627, 2017.

[9] M. Saidani, D. Saraireh, and M. Gerges, "Behaviour of different types of fibre reinforced concrete without admixture," *Engineering Structures*, vol. 113, pp. 328–334, 2016.

[10] A. Carpinteri, G. Fortese, C. Ronchei, D. Scorza, and S. Vantadori, "Mode I fracture toughness of fibre reinforced concrete," *Theoretical and Applied Fracture Mechanics*, vol. 91, pp. 66–75, 2017.

[11] W. Abbass, M. I. Khan, and S. Mourad, "Evaluation of mechanical properties of steel fiber reinforced concrete with different strengths of concrete," *Construction and Building Materials*, vol. 168, pp. 556–569, 2018.

[12] D. Y. Gao, L. P. Zhao, H. Feng, and S. B. Zhao, "Flexural toughness and it's evaluation method of steel fiber reinforce concrete," *Journal of Buliding Materials*, vol. 17, no. 5, pp. 783–789, 2014.

[13] H. Y. Pan and Y. C. Ma, "Impact resistance of steel fiber reinforced concrete and it's mechanism of crack resistance and toughening," *Journal of Buliding Materials*, vol. 20, no. 6, pp. 956–961, 2017.

[14] B. Li, L. Xu, Y. Shi, Y. Chi, Q. Liu, and C. Li, "Effects of fiber type, volume fraction and aspect ratio on the flexural and acoustic emission behaviors of steel fiber reinforced concrete," *Construction and Building Materials*, vol. 181, pp. 474–486, 2018.

[15] V. M. D. A. Monteiro, L. R. Lima, and F. D. A. Silva, "On the mechanical behavior of polypropylene, steel and hybrid fiber reinforced self-consolidating concrete," *Construction and Building Materials*, vol. 188, pp. 280–291, 2018.

[16] V. Marcos-Meson, A. Michel, A. Solgaard, G. Fischer, C. Edvardsen, and T. L. Skovhus, "Corrosion resistance of steel fibre reinforced concrete-A literature review," *Cement & Concrete Research*, vol. 103, pp. 1–20, 2017.

[17] M. Rangelov, S. Nassiri, L. Haselbach, and K. Englund, "Using carbon fiber composites for reinforcing pervious concrete," *Construction and Building Materials*, vol. 126, pp. 875–885, 2016.

[18] Y. Tong, X. Tian, C. J. Zhu, Y. Zeng, W. Y. Niu, and Q. Wang, "Experiments and analysis on mechanical strength of carbon fiber reinforced concrete," *Bulletin of The Chinese Ceramic Society*, vol. 34, no. 8, pp. 2281–2285, 2015.

[19] Z. Deng, "The fracture and fatigue performance in flexure of carbon fiber reinforced concrete," *Cement and Concrete Composites*, vol. 27, no. 1, pp. 131–140, 2005.

[20] X. C. Wang, L. Zhou, and J. W. Wang, "Method of surface treatment of carbon fiber and its evaluation," *Advanced Materials Research*, vol. 815, pp. 827–832, 2013.

[21] N. H. Liang, Y. Zhong, and X. R. Liu, "Experimental study of flexural toughness for multi-scale polypropylene fiber reinforced concrete," *Journal of Central South University (Science and Technology)*, vol. 48, no. 10, pp. 2783–2789, 2017.

[22] S. Yin, R. Tuladhar, T. Collister, M. Combe, N. Sivakugan, and Z. Deng, "Post-cracking performance of recycled polypropylene fibre in concrete," *Construction and Building Materials*, vol. 101, no. 1, pp. 1069–1077, 2015.

[23] F. Bauer, M. Kempf, F. Weiland, and P. Middendorf, "Structure-property relationships of basalt fibers for high performance applications," *Composites Part B: Engineering*, vol. 145, pp. 121–128, 2018.

[24] V. Fiore, T. Scalici, G. Di Bella, and A. Valenza, "A review on basalt fibre and its composites," *Composites Part B: Engineering*, vol. 74, pp. 74–94, 2015.

[25] A. Narayanan and P. Shanmugasundaram, "Evaluation of heat resisting behaviour of basalt fibre reinforced FG tiles," *Construction and Building Materials*, vol. 170, pp. 679–689, 2018.

[26] X. Sun, Z. Gao, P. Cao et al., "Fracture performance and numerical simulation of basalt fiber concrete using three-point bending test on notched beam," *Construction and Building Materials*, vol. 225, pp. 788–800, 2019.

[27] X. Sun, Z. Gao, P. Cao et al., "Mechanical properties tests and multiscale numerical simulations for basalt fiber reinforced concrete," *Construction and Building Materials*, vol. 202, pp. 58–72, 2019.

[28] J. Wang, Y. Ma, Y. Zhang, and W. Chen, "Experimental research and analysis on mechanical properties of chopped basalt fiber reinforced concrete," *Engineering Mechanics*, vol. 31, no. S1, pp. 99–102, 2014.

[29] S. J. Jin, Z. L. Li, J. Zhang, and Y. L. Wang, "Experimental study on anti-freezing and thawing performance of reinforced concrete of basalt fiber under corrosion condition," *Engineering Mechanics*, vol. 32, no. 5, pp. 178–183, 2015.

[30] Y. Yu, H. Zhu, X. C. Zhu, and Q. Huang, "Study on impact resistance of basalt fiber reinforced concrete," *Journal of Building Structures*, vol. 36, no. 2, pp. 354–358, 2015.

[31] J. Branston, S. Das, S. Y. Kenno, and C. Taylor, "Mechanical behaviour of basalt fibre reinforced concrete," *Construction and Building Materials*, vol. 124, pp. 878–886, 2016.

[32] C. High, H. M. Seliem, A. El-Safty, and S. H. Rizkalla, "Use of basalt fibers for concrete structures," *Construction and Building Materials*, vol. 96, pp. 37–46, 2015.

[33] X. Z. Wang, C. X. Li, J. Y. Ling, R. H. Yang, and H. L. Xie, "Experimental study on early crack of basalt fiber reinforced concrete," *Bulletin of the Chinese Ceramic Society*, vol. 36, no. 11, pp. 3860–3866, 2017.

[34] S. Xu, M. A. Malik, Q. Li, and Y. Wu, "Determination of double-K fracture parameters using semi-circular bend test specimens," *Engineering Fracture Mechanics*, vol. 152, pp. 58–71, 2016.

[35] Q. C. Xue, J. C. Zhang, J. He, Y. N. Li, T. J. Ramze, and Ermek, "Experimental study on fracture toughness of basalt fiber reinforced high strength concrete under three-point bending," *Concrete*, vol. 10, pp. 50–53, 2016.

[36] Q. C. Xue, J. C. Zhang, J. He, T. J. Ramze, and Ermek, "Experimental study of fracture properties for basalt-fiber-reinforced concrete," *Journal of Harbin Engineering University*, vol. 37, no. 8, pp. 1027–1033, 2016.

[37] J. Wang, J. H. Ren, and D. P. Guo, "Size effect of basic mechanical properties of chopped basalt fiber reinforced concrete," *Journal of Architecture and Civil Engineering*, vol. 32, no. 5, pp. 96–103, 2015.

[38] X. Liu and Z. Li, "Determining double-K fracture parameters of concrete only by the measured peak load," *Theoretical and Applied Fracture Mechanics*, vol. 85, pp. 412–423, 2016.

[39] S. Hu, X. Zhang, and S. Xu, "Effects of loading rates on concrete double- K fracture parameters," *Engineering Fracture Mechanics*, vol. 149, pp. 58–73, 2015.

[40] S. L. Xu, *Fracture Mechanics of Concrete*, Science publishing Company, Beijing, China, 2011.

[41] S. L. Xu, L. X. Dong, B. W. Wang, and Q. H. Li, "Development of concrete fracture mechanics in China during the past three decades," *Journal of Hydraulic Engineering*, vol. 45, no. S1, pp. 1–9, 2014.

[42] H. W. Reinhardt and S. Xu, "Crack extension resistance based on the cohesive force in concrete," *Engineering Fracture Mechanics*, vol. 64, no. 5, pp. 563–587, 1999.

[43] S. L. Xu, S. B. Xiong, H. D. Li, and Y. Lv, "Quantitative characterization and mechanism analysis on thickness-dependent size effect of concrete fracture," *China Civil Engineering Journal*, vol. 50, no. 5, pp. 57–71, 2017.

[44] S. L. Xu, *Standard Method for Fracture Testing and Determination of Fracture Toughness of Concrete*, Mechanical Industry Press, Beijing, China, 2009.

[45] G. Ruiz, J. J. Ortega, R. C. Yu, S. Xu, and Y. Wu, "Effect of size and cohesive assumptions on the double- K fracture parameters of concrete," *Engineering Fracture Mechanics*, vol. 166, pp. 198–217, 2016.

[46] S. Kumar, S. R. Pandey, and A. K. L. Srivastava, "Determination of double- K fracture parameters of concrete using peak load method," *Engineering Fracture Mechanics*, vol. 131, pp. 471–484, 2014.

[47] L. M. Wang, X. X. Ge, L. Liu, and D. H. Zhang, "Measurement on fracture process and analysis on mechanical performance of steel fiber reinforced concrete," *Journal of Hydraulic Engineering*, vol. 40, no. 8, pp. 995–1001, 2009.

[48] D. J. Zhang, S. L. Xu, and H. M. Hao, "Experimental study on fracture parameters of three-point bending beam based on smart properties of CFRC," *Journal of Hydroelectric Engineering*, vol. 2, pp. 71–77, 2008.

[49] P. Bernardi, E. Michelini, A. Sirico, S. Vantadori, and A. Zanichelli, "Fracture toughness of fibre-reinforced concrete determined by means of numerical analysis," *Procedia Structural Integrity*, vol. 5, pp. 848–855, 2017.

[50] Y. Chi, L. Huang, and M. Yu, "Calibration method of damage plasticity model for steel-polypropylene hybrid fiber reinforced concrete based on ABAQUS," *Engineering Mechanics*, vol. 34, no. 12, pp. 131–142, 2017.

[51] S. W. Hu and Z. X. Mi, "Numerical simulation of concrete crack propagation process on extended finite element method," *Journal of Hydraulic Engineering*, vol. 45, no. S1, pp. 51–56, 2014.

[52] S.-N. Roth, P. Léger, and A. Soulaïmani, "A combined XFEM-damage mechanics approach for concrete crack propagation," *Computer Methods in Applied Mechanics and Engineering*, vol. 283, pp. 923–955, 2015.

[53] G. F. Lu, Y. Liu, and C. L. Zhang, "Analysis of strain energy release rate based on virtual crack closure technique," *Acta Materiae Compositae Sinica*, vol. 26, no. 2, pp. 210–216, 2009.

[54] P. S. Valvo, "A physically consistent virtual crack closure technique for I/II/III mixed-mode fracture problems," *Procedia Materials Science*, vol. 3, pp. 1983–1987, 2014.

[55] Profession Standard of the electric power industry of the People's Republic of China, *DL/T 5332-2005 Norm for Fracture Test of Hydraulic Concrete*, China Electric Power Press, Beijing, China, 2005.

[56] Profession Standard of the People's Republic of China, *GB/T 17671-1999 Method of Testing Cements-Determination of Strength*, China Standards Press, Beijing, China, 1999.

[57] Profession Standard of the People's Republic of China, *GB/T 1346-2011 Test Methods for Water Requirement of Normal Consistency, Setting Time and Soundness of the Portland Cement*, China Standards Press, Beijing, China, 2011.

[58] Profession Standard of the People's Republic of China, *GB/T 1345-2005 the Test Sieving Method for Fineness of Cement*, China Standards Press, Beijing, China, 2005.

[59] Profession Standard of the People's Republic of China, *GB175-2007 Common Portland Cement*, China Standards Press, Beijing, China, 2007.

[60] Profession Standard of the electric power industry of the People's Republic of China, *DL/T 5055-2007 Technical Specification of Fly Ash for Use in Hydraulic Concrete*, China Electric Power Press, Beijing, China, 2007.

[61] Profession Standard of the electric power industry of the People's Republic of China, *DL/T 5100-2014 Technical Code for Chemical Admixtures for Hydraulic Concrete*, China Electric Power Press, Beijing, China, 2014.

[62] Profession Standard of the electric power industry of the People's Republic of China, *DL/T 5144-2015 Specifications for Hydraulic Concrete Construction*, China Electric Power Press, Beijing, China, 2015.

[63] Profession Standard of the electric power industry of the People's Republic of China, *DL/T5151-2014 Code for Testing Aggregates of Hydraulic Concrete*, China Electric Power Press, Beijing, China, 2014.

[64] Profession Standard of the People's Republic of China, *JGJ/T 22l-2010 Technical Specification for Application of Fiber Reinforced Concrete*, China Architecture & Building Press, Beijing, China, 2010.

[65] Profession Standard of the electric power industry of the People's Republic of China, *DL/T 5330-2015 Code for Mix Design of Hydraulic Concrete*, China Electric Power Press, Beijing, China, 2015.
[66] Profession standard of China Architecture & Building association, *CECS13:2009 Standard for Methods for Fiber Reinforced Concrete*, China Planning Press, Beijing, China, 2009.
[67] E. F. Rybicki and M. F. Kanninen, "A finite element calculation of stress intensity factors by a modified crack closure integral," *Engineering Fracture Mechanics*, vol. 9, no. 4, pp. 931–938, 1977.
[68] K. N. Shivakumar, P. W. Tan, and J. C. Newman Jr., "A virtual crack-closure technique for calculating stress intensity factors for cracked three dimensional bodies," *International Journal of Fracture*, vol. 36, no. 3, pp. 643–650, 1988.
[69] P. Cao, D. Feng, C. Zhou, and W. Zuo, "Study on fracture behavior of polypropylene fiber reinforced concrete with bending beam test and digital speckle method," *Computers and Concrete*, vol. 14, no. 5, pp. 527–546, 2014.
[70] Y. C. Sang, *Application of CZM and VCCT Methods in Crack Propagation Numerical Simulation*, Lanzhou University of Technology, Lanzhou, China, 2017.
[71] Profession Standard of the People's Republic of China, *GB 50010-2010 Code for Design of Concrete Structures*, China Building & Industry Press, Beijing, China, 2010.